Assessing the fate of slab-derived metallic melt in deep Earth through experimental investigation of its wetting behavior at high pressure

by

Junjie Dong
董 俊杰

A thesis submitted in partial fulfillment of the requirements for
the Degree of Bachelor of Science with Honors in
Earth and Environmental Sciences from the University of Michigan
2017

Thesis Advisor: Jie (Jackie) Li

Department of Earth and Environmental Sciences
University of Michigan
Ann Arbor
April 2017

Acknowledgements

First and foremost, I would like to thank my research and thesis advisor, Professor Jackie Li, who opened the door to mineral physics research for me and provided indispensable academic assistance and tremendous emotional support through the bumpy road to finish my research project and this thesis. To me, Jackie has been more than just a brilliant and prominent scientist, she is an approachable mentor, a creative inspiration and a considerate friend that instantly assures me that I am capable of achieving all my academic ambitions. It has been such a rewarding experience to have her guidance throughout my research and writing this thesis.

Besides, I must also thank my senior lab mate, Dr. Feng Zhu, for generously sharing his time and opinions with me for many constructive discussions that greatly help my research. I would also like to thank another fellow researcher, Dr. Jiachao Liu, for assistance with electron probe. In addition, I am indebted to the many established but amiable scientists who share their illuminating insights to this research. They include: Hidenori Terasaki, Shun-ichiro Karato, Wendy Mao, Carl Agee, Dave Stevenson and Dave Walker.

I finish with where the source of my spirit resides, my family in China. I feel extremely grateful for their unconditional love and wholehearted support to me and thank them for always standing by me whenever I needed it.

I wish the seed of the curiosity about the deep Earth sown in my mind would grow up into an oasis, I hope this is not just a wish!

Abstract

Metallic melt containing iron (Fe) and carbon (C) is likely present in subducted slabs at depths greater than 250 km inside the Earth. Depending on its wetting behavior, such dense melt may be trapped in the mantle or drain into the core. Here, high-pressure and high-temperature experiments were conducted to assess the fate of slab-derived metallic melt. At the conditions of the mid-mantle, between 10 and 23 GPa in pressure and 1600 and 1800 ˚C in temperature, the measured dihedral angles of Fe-C melt in olivine, ringwoodite, and bridgmanite-ferropericlase matrixes are 108˚ to 119°, well above the critical value of 60°. The large dihedral angles correspond to percolation threshold of at least 6%, which is the minimum melt fraction needed to develop long-range melt connectivity. This result implies that Fe-C melt in the mid-mantle is expected to occur as isolated pockets and will not percolate through silicate matrix to reach greater depths.

1. Introduction

Isotopic studies found that most of the Earth's core formed rapidly in the early stage of the Earth's history at about 4.5 billion years ago (e.g. Yin and Jacobsen, 2006). It is widely accepted that by about 4 billions years ago, the core has reached its current size and its growth ceased (Rubie et al., 2007). A number of recent studies, however, suggest that iron-rich alloys may be actively produced in the mantle, thus opening up the possibility of core-growth of the Earth through percolation at the present time. Previous studies suggest that the lower mantle is metal-saturated because bridgmanite can incorporate a significant amount of ferric iron (e.g. Frost et al., 2004). Rohrbach et al. (2007) showed that the deep parts of the upper mantle are likely metal-saturated as well because pyroxene and garnet can also incorporate ferric iron. Furthermore, they proposed that metallic iron may reduce subducted carbonates to produce elemental carbon or carbide. As a field evidence, iron carbide was found as inclusions in diamond from Juina, Brazil, which are thought to have originated in the mantle transition zone or the lower mantle (Kaminsky and Wirth, 2011). Taken together, these studies suggest that iron carbon mixtures are likely present in both the upper and lower mantle.

The hypothesis of on-going core growth has become particularly intriguing because recent studies suggested iron-carbon melt may form near the core-mantle boundary (e.g., Liu et al., 2016). If the iron-carbon melt remains trapped in the matrix of solid silicates or oxides, it may be returned to the shallower part of the mantle through global convection. Alternatively, the iron-carbon melt may percolate through the silicate or oxide and drain into the core. The latter scenario implies that the Earth's core is actively growing. Liu et al, (2016) proposed that some Ultra Low Velocity Zones (ULVZs) might be isolated patches containing iron-carbon

melts. They showed that the eutectic-melting curve of the Fe-C binary system crosses the mantle geotherm near the core-mantle boundary, and that the presence of Fe-C melt can explain seismically observed density and velocity features of such ULVZs.

In fact, the amount of density excess and velocity reductions partly depend on the wetting behavior of metallic melt on the solid matrix, especially for the reduction in shear wave velocity (V_S). In Liu et al. (2016)'s models, depending on the wetting behavior of the Fe-C melt in silicate matrix, the fraction of Fe-C in the ULVZs patches ranges from 5-11% to 9-16%. With large dihedral angle, the Fe-C melt is not wetting and has a higher percolation threshold. In this case, a relatively large-fraction of melt will be trapped in the mantle without draining into the core. If the dihedral angle is below the critical value of 60°, then the Fe-C melt will form connected network and eventually drain into the core. Knowledge of the wetting behavior of Fe-C is therefore critical for understanding the dynamic behavior of such ULVZs and predicting their fate. Draining of Fe-C melt would imply active core growth. With an estimated 1 wt.% Fe-C in the mantle (e.g. Wood et al., 2013), loss of Fe-C from 40% of the mantle corresponds to 0.8% growth in core mass at the expense of 0.4% reduction in mantle mass, which is equivalent to about 10km expansion in core radius over Earth's history.

In this study, we measure the dihedral angle of Fe-C melt in olivine polymorphs and bridgmanite at high pressures and high temperatures. The results are applied to test the hypothesis of on-going core growth through percolative drainage of iron-carbon alloys through the mantle into the core.

2. Methods

2.1 Experimental

Starting materials were mixtures of powdered San Carlos olivine and Fe-C. The natural olivine sample had an approximate composition of $(Mg_{0.9}Fe_{0.1})_2SiO_4$ and Fe-C powders contained 96 wt.% reduced Fe powder and 4 wt.% graphite. The silicate composition with Fe#=0.1 are applicable to the mantle composition of the Earth (e.g. Ringwood, 1991), and the Fe-C composition corresponds to its eutectic composition at 10 GPa (Fei and Brosh, 2014). The San Carlos olivine were ground to fine grains of 5-10 μm under ethanol in an agate mortar for one hour and dried at 100 °C before mixed with powdered Fe-C. The starting materials were fully packed into a sintered MgO capsule between two layers of fine MgO powder (a schematic configuration is shown in Fig. 1). The MgO capsule and powder were dried at 950 °C for approximately 2 hours to avoid trapped moisture before sample loading. The volume fraction of Fe-C in the loaded mixture was 3 vol.%, which is less than the melt fraction at the connection boundary where the percolation threshold is ~71° (von Bargen and Waff, 1986).

High pressure experiments were carried out using the 1000-ton Walker-type multi anvil press at the University of Michigan. Experiments at pressures up to 17 GPa used Toshiba-Tungaloy F-grade tungsten carbide (WC) cubes with 5mm truncation edge length (TEL) and those at pressures up 23 GPa used similar WC cubes with 3mm TEL. In addition, LaCrO3 heaters were used to minimize thermal gradient across the sample (Li et al., 2003). Temperature was monitored using the power curves determined by previous multi-anvil experiments with

$W_{97}Re_3$-$W_{75}Re_{25}$ thermocouples for. Pressure uncertainty is estimated within ± 5% on basis of duplication experiments and does not include the effect of temperature. More experimental setup and calibration details were discussed in Li and Li (2015).

In all experiments, the sample was first pressurized at 5 GPa and then sintered for 8-12 hours during the compression process to the target pressures. Target temperatures were located below the melting temperatures of the silicate phases and above the melting temperatures of the iron-rich mixture. Until quenched by cutting power to the heater, target pressures and temperatures in all experiments were maintained for approximately 30 mins. In the previous studies of the silicate-Fe-melt system, the time scale of the textural equilibrium was reported to be from 12 minutes at 25 GPa and 2500 K (Takafuji et al., 2004) to 50 minutes at 14 GPa and 1700 ºC (Shannon, 1998). We suggest that 30 minutes is long enough to establish a local textural equilibrium existed at the interface which allows reproducible dihedral angle measurements.

2.2 Analytical

Recovered run products were mounted in epoxy, aluminum-coated, sectioned and polished for composition and texture analyses using a JOEL 700FLV field emission SEM and a CAMECA SX100 electron microprobe in the Central Campus Electron Microbeam Analysis Laboratory (EMAL) at the University of Michigan. Currently, the carbon content of quenched iron liquid was estimated using electron dispersive spectra (EDS) data. Electron probe measurement on quenched iron melt and solid matrixes are to be performed. Identification of the silicates phases in the recovered runs were conducted using a Renishaw inVia confocal Raman microscope.

Apparent dihedral angles were measured from back scattered electron (BSE) images of the recovered sample by using the thresholding and protractor functions of the image processing software ImageJ. As a mean to establish a consistent criterion and hence to increase reproducibility of dihedral angle measurement, the BSE images of the measured areas were processed by the "thresholding" function by ImageJ (Fig. 2, Perez and Pascau, 2013). Each individual dihedral angle was measured by the "protractor" function in ImageJ. The true dihedral angles were taken to be the median value of the apparent dihedral angle distribution, so-called "effective dihedral angle" (Stickels and Hucke, 1964). The measurement error of the dihedral angle is based on ± 10° around the population median (e.g. Jurewicz and Jurewicz, 1986; Holness, 2010). Between 91 and 257 measurements were conducted in this study. It is possible that a small amount of dihedral angle measurements (<~100) can be inadequate to determine the effective dihedral angles reproducibly.

3. Results and discussion

At the pressure and temperature conditions of all experiments, the Fe-C melt formed pockets at the grain boundaries of silicate/oxide matrix (Fig. 3), and the original phase of San Carlos olivine recrystallized to form olivine at 10 GPa, ringwoodite at 17 GPa and bridgmanite-ferropericlase at 23 GPa (Fig. 4). The quenched Fe-C melt assumed relatively spherical shape and froze into interspersed carbon-rich and carbon-poor domains with characteristic dendritic texture (Fig. 5). Most of the quenched melt consists dominantly of Fe and C, with minor amount of Ni and O that may come from natural sample starting materials (Fig. 6b). The

median values of the dihedral angles of Fe-C melt in olivine, ringwoodite, and bridgmenite-ferropericlase are 116 ° at 10 GPa, 119 ° at 17 GPa and 108° at 23 GPa, respectively (Table 1).

3.1 Dihedral angle and percolation

The underlying theory of wetting phenomena, which relates grains, phases and interfaces, has been well developed for the ideal case of an isotropic system to interpret rock microstructures: The feasibility of percolation is determined by the ratio of the solid-liquid interfacial energy (γ_{ss}) and the solid-solid interfacial energy (γ_{sl}) (Fig. 7), If the two grains of solid phases are the same material and isotropic, then the equation above can be simplified to (e.g. Porter, 1983):

$$\frac{\gamma_{ss}}{\gamma_{sl}} = 2\cos\frac{\theta}{2}$$

A dihedral angle of $\theta = 60°$ or less leads to the formation of an interconnected network of liquid regardless of the melt fraction, whereas a dihedral angle θ that is greater than 60° implies that a significant fraction of iron melt may be stranded as isolated pockets.

3.2 Effect of pressure on dihedral angle

The results from this study show little pressure dependence of the dihedral angle θ between 10 to 23 GPa (Fig. 8a). A small reduction in the effective dihedral angle from 119° at 17 GPa to 108° at 23 GPa falls within the measurement uncertainty of approximately ±10°. Literature data at lower pressure show that Fe-C melt with 4.3 wt.% carbon at 3 GPa and 1400 °C has an effective dihedral angle of 115° (Duncan and Fei, 2017), which corresponds to the dihedral angles of Fe-C melt measured in this study at higher pressures. Studies on Fe-Si melt

up to 47 GPa and 3000 K (Takafuji et al., 2004) and the Fe-S melt up to 64 GPa and 3300 K (Shi et al., 2013), however, demonstrated that at higher pressures the dihedral angles of molten iron-alloys in bridgmanite matrix decreased with the increasing pressures and temperatures and would reach the critical value of 60 ° (Fig. 8b).

The lack of pressure dependence for the dihedral angle of Fe-C melt in silicate is as expected from the known wetting behavior at 1 bar and theoretical understanding of interfacial thermodynamics. The change of interfacial energy between melt and solid (γ_{ss}) at a given temperature (T) can be described by the Gibbs adsorption isotherm (Lyklema, 2000):

$$d\gamma = \delta dP - \sum \Gamma_i d\mu_i$$

where δ is the thickness of the interface between melt and solid, P is pressure, Γ_i is surface excess concentration per unit area, and μ_i is chemical potential of component i in the melt. The pressure dependence of interfacial energy between melt and solid (γ_{sl}) at a given composition (μ) and temperature (T) can be derived by applying the Gibbs-Duhem relation (Everett, 1987), which results in

$$\frac{d\gamma}{dP} = \delta - \Gamma_{melt} V_{melt}$$

Where V_{melt} represents the partial molar volume of the melt. At the ambient pressure and 1843 K, the surface excess of sulfur (Γ_{Fe-S}) is $11.6\times10^{-6} mol\ m^{-2}$ in iron-rich melt containing ~0.1wt. % sulfur (Halden and Kingery, 1955). Both values are positive and the $\Gamma_{melt} V_{melt}$ term is much larger than the thickness of the interface, typically a few times of lattice spacings (e.g. Woodruff, 1973), and therefore result in negative pressure dependence of the interfacial energy. Assuming the interfacial energy between solid grains (γ_{ss}) is less sensitive to pressure, a reduction in γ_{sl} will lead to smaller dihedral angle. In comparison, the surface excess of carbon in iron-rich melt is virtually zero, implying no pressure effect. If the

adsorption behaviors of these elements behave in the same way at high pressures, the dihedral angle of Fe-S melt will have a strong negative pressure dependence while that of Fe-C melt will not be affected by compression. This simplified relation can explain the wetting behavior of Fe-S melts at high pressures (e.g., Shi et al., 2013), and the results on Fe-C melt from this study.

3.3 Effect of melt composition on dihedral angle

The dihedral angle of iron-rich melt in silicate is influenced by the presence of alloying elements such as O, S, and Si (e.g. Takafuji et al., 2004; Mann et al., 2008; Terasaki et al., 2008). For example, adding oxygen to an Fe-S melt lowers its dihedral angles in silicate matrix, which could fall below the critical value of 60 ˚at sufficiently high oxygen concentrations (Terasaki et al., 2008). Other non-metal elements, such as S (e.g. Terasaki et al., 2005), Si (e.g. Mann et al., 2007) and P (e.g. Terasaki et al., 2007) can also reduce the dihedral angle of iron-rich melt in silicate, although the effect is weaker than oxygen.

At the ambient pressure, the surface tension of iron-rich liquid can be measured experimentally in Halden and Kingery (1955). It demonstrates that, at the ambient pressure and 1843 K, adding 0.1 wt.% oxygen rapidly decrease the surface tension of liquid iron by about 35% and adding the same amount of sulfur liquid iron has smaller decrease in surface tension. Instead the addition of carbon in iron-rich alloy has no effect on its surface tension. Even though the dihedral angle of iron-rich melt at high pressures and temperatures is characterized by the interfacial energy between iron liquid and the silicate matrix, which is different from most metallurgical studies. The general trend of surface energy decrease by

adding certain amounts of light elements (e.g., oxygen, sulfur and carbon) holds in both case if we assume the solid phases would not contribute to the shape of iron melt significantly.

An oxidized starting materials or moistures trapped in the capsule might introduce excess oxygen in the melt during experiment. The ex-solution of FeO component when the liquid was quenched formed tiny blobs in the iron-rich melt phase in Terasaki et al. (2005). In this study, no tiny blob was observed within Fe-C melt phase. We assumed the oxygen content of the Fe-C melt was minimized and did not contribute to the dihedral angles of iron-rich melt in all experiments. However, the oxygen solubility in the liquid decreases dramatically upon quenching (Naldrett, 1969) and the oxygen dissolved in the iron-rich melt will not be preserved completely in the recovered samples and hence remains difficult to determine accurately.

3.4 Effect of crystalline structure on dihedral angle

In this study on the dihedral angles of Fe-C melt, the silicate matrix recrystalized to form olivine at 10 GPa, and ringwoodite at 17 GPa. At a higher pressure of 23 GPa, bridgmanite and ferropericlase were formed due to the complete break-down of ringwoodite (Fig. 6a). Therefore, the solid phase transition, olivine and its polymorphs, at 10 and 17 GPa, and bridgmanite and ferropericlase at 23 GPa may affect the wetting behavior of iron-rich melt. The measured effective dihedral angles of Fe-C melt on different silicates and/or oxides over the pressure range from 10 to 23 GPa do not show a significant change and remained at about 115 °. In Shannon and Agee (1998), however, an abrupt drop in dihedral angle was observed after the lower mantle phase transition, which does not agree with this study. The dihedral angle of Fe-S melt drops from approximately 108 ° at upper mantle conditions to 71 ° at 25

GPa. This discrepancy may arise from the compositional effect where carbon and sulfur possess dissimilar adsorption behaviors. However, since their experiments were carried out with natural chondrite materials and using a different heating procedure from this study (completely melting the sample at a higher temperature and then cooling back below the silicate solidus), presence of the solid phases other than silicates and oxides and higher experimental temperature may explain this different observation. In addition, it is not known how the dynamics of the lower mantle transition (e.g grain size decrease and grain boundary change) contribute to the dihedral angle of iron-rich melt. In this study, bridgmanite and ferropericlase broken down from ringwoodite were the solid phases to model the major mineral assemblage of Earth's lower mantle. The additional ferropericlase phase may interact with iron-rich melt. Otsuka and Karato (2012) reported that ferropericlase (Mg,Fe)O in contact with iron-rich liquids leads to a morphological instability, causing blobs of iron-rich melt to wet the oxides without forming an interconnected network. If this morphological instability, indeed, exists in other Fe-rich melt like Fe-C and Fe-S, it will change the wetting behavior of the Fe-C melt in the bridgmanite-ferropericlase matrix. In this study, however, presence of ferropericlase at the lower mantle conditions due to the break-down reaction does not seem to change the dihedral angle measurement. In the run without break-down of ringwoodite at 17 GPa, a trace amount of ferropericlase was also observed and it might result from buffer reactions reported in some previous studies (Terasaki et al, 2005). Because the unexpected ferropericlase were a minor phase and not contact with Fe-C melt directly in that sample, we suggest that its presence would not affect the dihedral angle measurement significantly.

When the percolation model for core formation was first proposed, it requires that the matrix is a single isotropic solid phase. However, most mantle silicates are anisotropic and the

simplified surface energy relation defining the dihedral angles $cos\frac{\theta}{2} = \frac{\gamma_{ss}}{\gamma_{sl}}$ does not hold accurately and wetting behavior is more complicated than can be expressed by a single dihedral angle value. In an isotropic solid matrix, interconnectivity of the melt can form when the dihedral angle of the melt phase is below the critical value of 60°. Laporte and Watson (1995) showed that, however, a sufficiently high anisotropy of γ_{sl} may prompt the same melt phase to form plane-faced pockets isolated at grain corners. The wetting behavior of melt is fairly sensitive to $\frac{\gamma_{ss}}{\gamma_{sl}}$ (to a lesser extent γ_{ss}), depending on the lattice orientation of its surrounding grains to the grain boundary. Few experimental studies on the anisotropy of γ_{sl} within the olivine-basalt interface at low pressures were carried out but the iron-rich-melt system remains unknown. (e.g. Schäfer and Foley, 1997)

3.5 Effect of temperature on dihedral angle

The temperature effect on dihedral angle has been little studied at high pressures, but temperature dependence of surface energies of iron alloys was observed in some metallurgical studies (e.g. Passerone and Sangiorgi, 1984). It demonstrates that in eutectic systems surface energy decreases with increasing temperature monotonically, but not linearly. The dihedral angle of the melt phase drops to zero at a temperature below the melting point of the solid matrix. In Shannon and Agee (1998), the experiment on Fe-S melt at 25 GPa was pressurized and heated up to a temperature just below the silicate solidus and showed a significant dihedral angle drop from the experiments at lower pressures. This experiment at ~25 GPa was, indeed, run at the sub-solidus temperature of the silicate $(Mg_{0.76}Fe_{0.24})SiO_3$, and the abrupt reduction on dihedral angle of Fe-S melt reported may be possibly explained by the singular temperature effect at the sub-solidus temperature of the solid matrix. A similar

temperature effect on Fe-Si melt was reported in Takafuji et al. (2004), where the effective dihedral angle at 25 GPa decreases from 94 ° at 2400 K to 70 ° at 2800 K. Similarly, the large drop in dihedral angle was observed at a temperature close to the solidus of the silicate matrix $(Mg_{0.9}Fe_{0.1})SiO_3$, which may also result from the sub-solidus temperature effect.

In this study, the Fe-C melt were investigated at different pressure conditions close to the eutectic temperature, which ensured the iron alloys were fully molten. The run temperatures were far below the solidus of the silicate matrixes. No apparent temperature effect was observed over this upper mantle pressures between 1600 ºC and 1800 ºC. If the wetting behavior of iron-rich melt, indeed, will be affected significantly only at a sub-solidus temperature, it's likely that Fe-C melt behave as same as Fe-S and Fe-Si and decreases its dihedral angles on the silicate matrix right below the silicate solidus.

In the deep Earth, the combined effect of pressure and temperature makes difficult for us to investigate either of them constrained by reliability of phase diagram. The target temperature for experiments has to fall within the temperature interval beyond the liquids of iron-rich melt and below the solidus of silicates. It narrows down the temperature regime we are able to investigate while this small temperature regime shifts as pressure increases which also makes difficult investigating the pressure effect at same temperature.

3.6 Percolation threshold and connectivity

The dihedral angles of Fe-C melt on silicate matrix from 4 to ~23 GPa are well above the critical value of 60º and are not able to form an interconnected network, percolating through the silicates matrix with an estimated 3 vol.% melt. In fact, an increasing melt fraction is

likely to facilitate the wetting of iron-rich melt on its solid phase so that the interconnected network can form when the dihedral angle is still above the critical value of 60 °. The relation between percolation threshold and melt fraction was estimated for homogenously distributed melt on solid matrix by von Bargen and Waff (1986):

$$f_p \approx 0.009\sqrt{(\theta - 60)}$$

Where f_p is the percolation threshold for melt fraction and this relation holds if $60 \leq \theta \leq 100$ (e.g. Stevenson, 1986). In our runs except M063016, Fe-C melt is estimated to be 3 vol.% and it corresponds to a percolation threshold of ~71°, which is far below the measured dihedral angles of Fe-C melt in this study.

Jurewicz and Jones (1995) carried out a series of electrical conductivity experiments with iron-rich melt in silicates at subsolidius temperature and reported approximately 20 vol.% iron melt allowed detection of electrical signal due to connectivity. In M060316 the melt fraction of Fe-C was increased to more than 20 vol.% to compare with other experiments with estimated 3 vol.% of Fe-C melt. The Fe-C melt in M060316 shows less spherical shape but still does not form a long-distance connectivity (Fig. 5). It is clear that a significant amount of iron-rich melt changes the topology of mantle silicates with iron melt, however, the 20 vol. % of Fe-C melt was shown to be still not enough to form interconnected network to percolate through the bridgmanite-ferropericlase matrix. Frost et al. (2004) estimated up to ~1 wt. % metallic iron is likely to present in the deep mantle, which is far below the percolation threshold of at least 20 vol. % we observed in the experiment M060316. Therefore, Fe-C melt present in the deep mantle will be well trapped and is not able to percolate into the core.

3.7 Percolation-enabling mechanisms

The average value of 115° for the dihedral angle of Fe-C melt in mantle matrix does not allow an on-going core growth at upper mantle pressures. Multiple percolation-enabling mechanisms for iron-rich melt in silicates matrix were proposed, including partially molten silicates (e.g., Duncan and Fei, 2017) and shear deformation (e.g., Karato, 2011).

Partial molten silicates do not show strong evidence of decreasing dihedral angles of iron-rich melt and hence facilitate its percolation (e.g. Holzheid, 2013). However, if silicate melt is present in a large amount and significantly more than iron-rich melt. It may form discrete droplets within silicate melt and be separated from solid silicate phases due to density contrast. The wetting behavior of Fe-S-C melt from partial molten silicates was recently studied at 1-3 GPa and was found to be feasible when the amount of silicate melt is high enough to create channels that allow Fe-S-C melt to contribute to the core formation process (Duncan and Fei, 2017). However, the present-day mantle geotherm is not high enough to sustain a large amount of partial molten silicates, and therefore percolation of iron-rich melt with assistance of partial molten silicates is not likely to occur.

The dihedral angle of iron-rich melt on silicates with shear deformation was proposed as potential percolation mechanism for planetary core formation but it was barely studied due to experimental difficulty and less theoretical knowledge. Few deformation studies report the permeability of Fe-S melt under shear deformation are the same within uncertainty and do not exhibit a change with increasing deformation (e.g. Todd et al., 2016). Most likely, the effect of shear deformation also depends on the melt fraction, and the influence of shear deformation on the wetting behavior of iron-rich melt is small for a small melt fraction

(Karato, 2011). Therefore, without presence of enough melt, Fe-C melt will not be able to percolate through the silicate/oxide matrix to drain into the core nowadays.

4. Implications for mantle heterogeneity and core growth

Core-mantle segregation represents one of the most important differentiation events in Earth's history. The process of core formation likely consists of a series of events, starting as early as 5 million years after the origin of the solar system and possibly continuing to the present day (e.g., Vidal and Dosso, 1978; Liu et al, 2016). Previous quench experiments (e.g., Shannon and Agee 1998) and a recent synchrotron transmission x-ray microscopy study (Shi et al. 2013) on Fe-C melt found a critical reduction in the dihedral angle from the conditions of the Earth's upper mantle to that of the lower mantle. The results imply that Fe-rich melt is likely to percolate through the lower mantle efficiently to join the core. However, the dihedral angle of Fe-C melt remains well above the critical value of percolation up to 23 GPa and it indicates percolation of Fe-C melt would not be efficient enough as a core formation mechanism and the iron melt with presence of carbon produced in the mantle would be well trapped without drainage into the core to sustain an on-going core growth.

As discussed above, however, the quenched iron-rich liquid discovered in diamond inclusions consists not only Fe and C but also S and H (Smith et al. 2016). Meanwhile, light elements in core materials possibly consists like O, Si, S and H besides C (e.g. Poirier, 1994). Since dihedral angles of the iron-rich melt depend on its composition, the combinations of carbon and hydrogen, carbon and sulfur, or carbon, sulfur and hydrogen are all candidates of iron-rich melt that are likely present in the deep mantle. The decrease in interfacial energy of iron liquid with addition of sulfur is significant and may be able to reduce its dihedral angle below

the critical value of 60°. In addition, the wetting behavior of iron-rich melt with hydrogen still remains not known. It is possible that the dihedral angle of Fe-C melt with addition of S and/or H is lower or close to the critical value of percolation, which allows an on-growing core growth. We may note that the combination of carbon and oxygen is unlikely in this case. Their presences require different redox environments and they are expected to be mutually exclusive in iron-rich melt.

The possible sub-solidus temperature effect discussed above may not influence the wetting behavior of iron-rich melt present in the present-day mantle and hence enable the on-going core growth. It is due to a lower temperature constrained by the present geotherm. However, it may have a significant implication at core-mantle boundary. Iron enrichment is proposed to explain low seismic wave velocities and high electrical conductivity at the bottom of the mantle (e.g. Liu et al. 2016). According to Liu et al. (2016)'s model, if the Fe–C melt does not wet the grain boundaries, then as much as 9 vol.% melt would be required to reproduce the ULVZ seismic observed properties. To sustain a large amount of iron-rich melt at the lowermost of the Earth's mantle, Otsuka and Karato (2009) reported that the iron-rich melt completely wets the grain boundaries of ferropericlase and proposed another possible mechanism of morphological instability between iron-rich melt and ferropericlase to explain the seismic observation of ULVZs. As discussed above, similar sub-solidus temperature effects were reported on Fe-S and Fe-Si in silicate matrixes at about 25 GPa. Since across the core-mantle boundary region, the temperature jump is estimated to be over 1500 K, which allows the silicates at the lowermost mantle to be heated up close to a temperature just below its solidus, it implies iron-rich melt may be able to wet two major phases at the lowermost part of Earth's mantle and it may help explain large velocity reductions and high electrical conductivities of some regions in the D" layers. Further studies of this proposed sub-solidus

temperature effect will help us to understand the chemical heterogeneity of the core-mantle boundary including the Ultra Low Velocity Zone that still remains enigmatic.

5. Conclusions

Experiments showed that effective dihedral angles between silicates and Fe-C melt remain a similar value of ~115° at 10 to 23 GPa. There is no measureable pressure on the dihedral angles of Fe-C melt over this pressure range. The results combined with previous studies on silicates and oxides imply that dihedral angles of iron-rich melt through the mantle pressures up to 23 GPa are well above the percolation threshold. Percolation of Fe-C melt on silicate matrix is not feasible at upper mantle pressures of the Earth. Fe-C melt remains trapped in the matrix of solid silicate or oxide at upper mantle and may be returned to the shallower part of the mantle through global convection. However, that the iron-rich melt may percolate through the silicate or oxide is not ruled out with addition of other light elements present in the Earth's mantle.

References

Bargen, Nikolaus, and Harve S Waff. 1986b. “Permeabilities, Interfacial Areas and Curvatures of Partially Molten Systems: Results of Numerical Computations of Equilibrium Microstructures.” Journal of Geophysical Research: Solid Earth 91 (B9): 9261–76.

Duncan, M S, and Y Fei. 2017a. “Experimental Constraints on Metal Percolation Through Silicate: Implications for Core Formation on Asteroids and Planetesimals.” Lunar and Planetary Science Conference 48 (March). Lunar and Planetary Science Conference.

Everett, D.H., 1987. Application of thermodynamics to interfacial phenomena. Pure and applied chemistry, 59(1).

Fei, Yingwei, and Eli Brosh. 2014. “Experimental Study and Thermodynamic Calculations of Phase Relations in the Fe–C System at High Pressure.” Earth and Planetary Sceicens Letters. 408 (December): 155–62.

Frost, Daniel J, Christian Liebske, Falko Langenhorst, Catherine A McCammon, Reidar G Trønnes, and David C Rubie. 2004. “Experimental Evidence for the Existence of Iron-Rich Metal in the Earth's Lower Mantle.” Nature 428 (6981). Nature Publishing Group: 409–12.

Frost, Daniel J, Yuki Asahara, David C Rubie, Nobuyoshi Miyajima, Leonid S Dubrovinsky, Christian Holzapfel, Eiji Ohtani, Masaaki Miyahara, and Takeshi Sakai. 2010. “Partitioning of Oxygen Between the Earth's Mantle and Core.” Journal of Geophysical Research 115 (B2): 91.

Halden, F.A. & Kingery, W.D., 1955. Surface Tension at Elevated Temperatures. II. Effect of C, N, O and S on Liquid Iron Surface Tension and Interfacial Energy with Al 2O 3. The Journal of Physical Chemistry, 59(6), pp.557–559.

Holness, M B. 2010. “Decoding Dihedral Angles in Melt-Bearing and Solidified Rocks.” Journal of the Virtual Explorer 35.

Holzheid, A. (2013). Sulphide melt distribution in partially molten silicate aggregates: implications to core formation scenarios in terrestrial planets. European Journal of Mineralogy, 25(3), 267-277.

Jurewicz, Stephen R, and Amy J G Jurewicz. 1986. “Distribution of Apparent Angles on Random Sections with Emphasis on Dihedral Angle Measurements.” Journal of Geophysical Research: Solid Earth 91 (B9): 9277–82.

Jurewicz, S.R., Jones, J.H., 1995. Preliminary results of olivine/metal wetting experiments and the direct measurement of metal phase interconnectivity. Lunar Planet. Sci. XXVI, 709–710.

Kaminsky, Felix V, and Richard Wirth. 2011. “Iron Carbide Inclusions in Lower-Mantle Diamond From Juina, Brazil.” The Canadian Mineralogist 49 (2). The Canadian Mineralogist: 555–72.

Karato, S. I. (2012). Deformation of earth materials: an introduction to the rheology of solid earth. Cambridge University Press.

Laporte, D. & Watson, E.B., 1995. Experimental and theoretical constraints on melt distribution in crustal sources: the effect of crystalline anisotropy on melt interconnectivity. Chemical Geology, 124(3-4), pp.161–184.

Li, Jie, Chris Hadidiacos, Ho-Kwang Mao, Yingwei Fei, and Russell J Hemley. 2010. “Behavior of Thermocouples Under High Pressure in a Multi-Anvil Apparatus.” High Pressure Research 23 (4). Taylor & Francis Group: 389–401.

Li, Zeyu, and Jie Li. 2015. “Melting Curve of NaCl to 20 GPa From Electrical Measurements of Capacitive Current: American Mineralogist.” American Mineralogist.
Liu, Jiachao, Jie Li, Rostislav Hrubiak, and Jesse S Smith. 2016. “Origins of Ultralow Velocity Zones Through Slab-Derived Metallic Melt.” Proceedings of the National Academy of Sciences 113 (20). National Acad Sciences: 5547–51.
Lyklema, Johannes. Fundamentals of interface and colloid science: solid-liquid interfaces. Vol. 3. Academic press, 2000.
Mann, Ute, Daniel J Frost, and David C Rubie. 2008. “The Wetting Ability of Si-Bearing Liquid Fe-Alloys in a Solid Silicate Matrix—Percolation During Core Formation Under Reducing Conditions?” Physics of the Earth and Planetary Interiors 167 (1-2): 1–7.
Naldrett, A.J., 1969. A Portion of the System Fe-S-O between 900 and 1080 C and its Application to Sulfide Ore Magmas. Journal of Petrology, 10(2), pp.171–201.
Otsuka, K. & Karato, S.-I., 2012. Deep penetration of molten iron into the mantle caused by a morphological instability. Nature, 492(7428), pp.243–246.
Passerone, A. & Sangiorgi, R., 1985. Solid-Liquid Interfacial Tensions by the Dihedral Angle Method. a Mathematical Approach. Acta Metallurgica, 33(5), pp.771–776.
Pérez, J. M. M., & Pascau, J. (2013). Image processing with ImageJ. Packt Publishing Ltd.
Porter, D. A., Easterling, K. E., & Sherif, M. (2009). Phase Transformations in Metals and Alloys, (Revised Reprint). CRC press.
Ringwood, A E. 1991. “Phase Transformations and Their Bearing on the Constitution and Dynamics of the Mantle.” Geochim Cosmochim … 55 (8): 2083–2110.
Rohrbach, Arno, Chris Ballhaus, Ute Golla Schindler, Peter Ulmer, Vadim S Kamenetsky, and Dmitry V Kuzmin. 2007. “Metal Saturation in the Upper Mantle.” Nature 449 (7161). Nature Publishing Group: 456–58.
Rubie, D.C., Nimmo, F. & Melosh, H.J., 2015. Formation of the Earth's Core. In Treatise on Geophysics. Elsevier, pp. 43–79.
Schäfer, Frank N, and Stephen F Foley. 1997. “The Effect of Crystal Orientation on the Wetting Behaviour of Silicate Melts on the Surfaces of Spinel Peridotite Minerals.” Contributions to Mineralogy and Petrology 143 (2). Springer-Verlag: 254–62.
Shannon, Margarita Catherine. 1998. Percolation of Iron Melts Through Mantle Minerals at High Pressure: Implications for Core Formation. ProQuest Dissertations and Theses; Thesis (Ph.D.)-Harvard University, 1998.
Shannon, M.C. & Agee, C.B., 1998. Percolation of Core Melts at Lower Mantle Conditions. Science, 280(5366), pp.1059–1061.
Shi, Crystal Y, Li Zhang, Wenge Yang, Yijin Liu, Junyue Wang, Yue Meng, Joy C Andrews, and Wendy L Mao. 2013a. “Formation of an Interconnected Network of Iron Melt at Earth/'S Lower Mantle Conditions.” Nature Geoscience 6 (11). Nature Research: 971–75.
Smith, C S. 1948. “Grains, Phases, and Interphases: an Interpretation of Microstructure.” Trans. Metall. Soc. AIME, Vol. 175, P. 15-51 (1948). 175. Trans. Metall. Soc. AIME: 15–51.
Smith, Evan M, Steven B Shirey, Fabrizio Nestola, Emma S Bullock, Jianhua Wang, Stephen H Richardson, and Wuyi Wang. 2016. “Large Gem Diamonds From Metallic Liquid in Earth’s Deep Mantle.” Science 354 (6318): 1403–5.
Stevenson, D J. 1986. “On the Role of Surface Tension in the Migration of Melts and Fluids.” Geophysical Research Letters 13 (11): 1149–52.
Stickels, C A, and E E Hucke. 1964. Measurement of Dihedral Angles. Transactions of the Metallurgical Society of AIME.

Takafuji, Naoto, Kei Hirose, Shigeaki Ono, Fangfang Xu, Masanori Mitome, and Yoshio Bando. 2004a. “Segregation of Core Melts by Permeable Flow in the Lower Mantle.” Earth and Planetary Sciences Letters. 224 (3-4): 249–57.

Terasaki, Hidenori, Daniel J Frost, David C Rubie, and Falko Langenhorst. 2005. “The Effect of Oxygen and Sulphur on the Dihedral Angle Between Fe–O–S Melt and Silicate Minerals at High Pressure: Implications for Martian Core Formation.” Earth and Planetary … 232 (3-4): 379–92.

Terasaki, H., Frost, D. J., Rubie, D. C., & Langenhorst, F. (2007). Interconnectivity of Fe–O–S liquid in polycrystalline silicate perovskite at lower mantle conditions. Physics of the Earth and Planetary Interiors, 161(3), 170-176.

Terasaki, Hidenori, Daniel J Frost, David C Rubie, and Falko Langenhorst. 2008. “Percolative Core Formation in Planetesimals.” Earth and Planetary Sciences Letters. 273 (1-2): 132–37.

Todd, K. A., Watson, H., Yu, T., & Wang, Y. (2016). The effects of shear deformation on planetesimal core segregation: Results from in-situ X-ray micro-tomography. American Mineralogist, 101(9), 1996-2004.

Vidal, Philippe, and Laure Dosso. 1978. “Core Formation: Catastrophic or Continuous? Sr and Pb Isotope Geochemistry Constraints.” Geophysical Research Letters 5 (3): 169–72.

Wood, B J, J Li, and A Shahar. 2013. “Carbon in the Core: Its Influence on the Properties of Core and Mantle.” Rev Mineral Geochem.

Wood, Bernard J, Michael J Walter, and Jonathan Wade. 2006. “Accretion of the Earth and Segregation of Its Core.” Nature 441 (7095). Nature Publishing Group: 825–33.

Woodruff, D. P. (1973). The solid-liquid interface. Cambridge University Press.

Yin, Qingzhu, S B Jacobsen, K Yamashita, J Blichert-Toft, P Télouk, and F Albarède. 2002. “A Short Timescale for Terrestrial Planet Formation From Hf-W Chronometry of Meteorites.” Nature 418 (6901). Nature Publishing Group: 949–52.

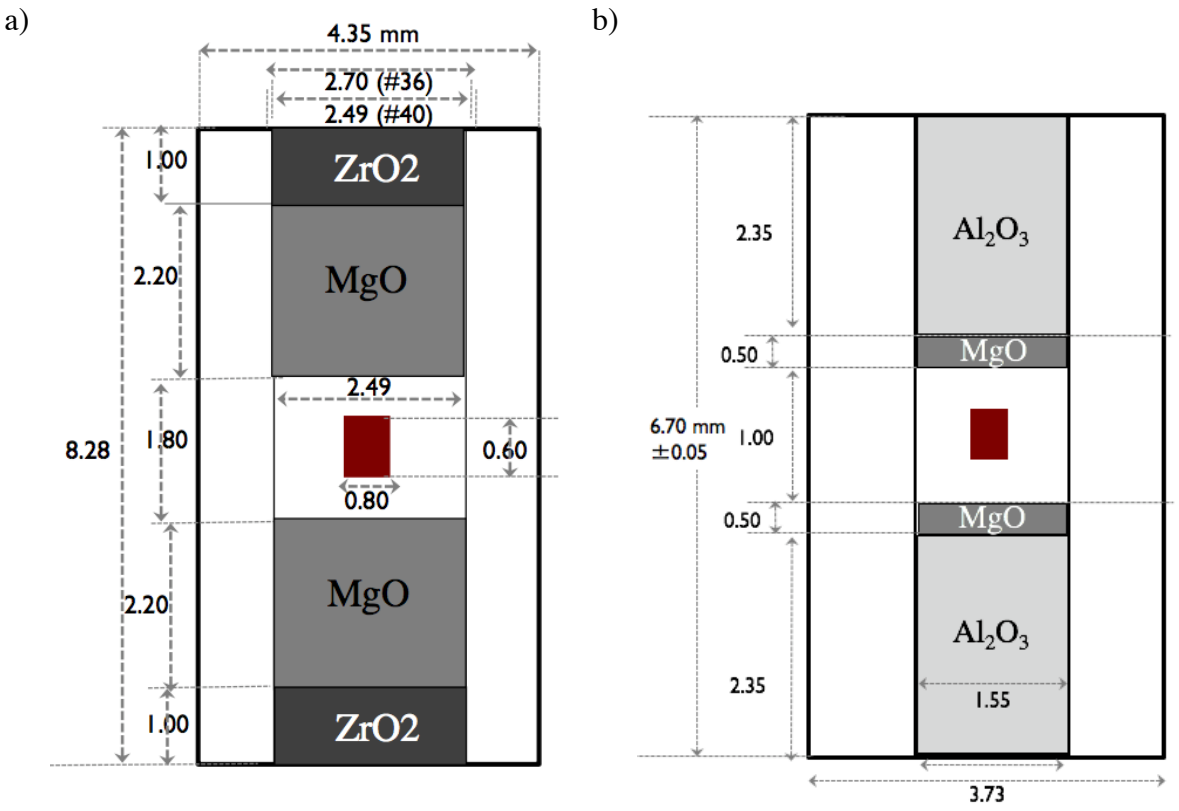

Fig. 1 Configurations of cell assemblies for high-pressure experiments

(a) cross-section of modified COMPRES 10/5 mm assembly showing the sample (red) in an MgO container (white), MgO spacers (gray) and zircon end-plugs (dark).

(b) cross-section of modified COMPRES 8/3 mm assembly showing the sample (red) in an MgO container (white), which is surrounded by an alumina sleeve (light gray), and MgO spacers (gray).

a)

b)

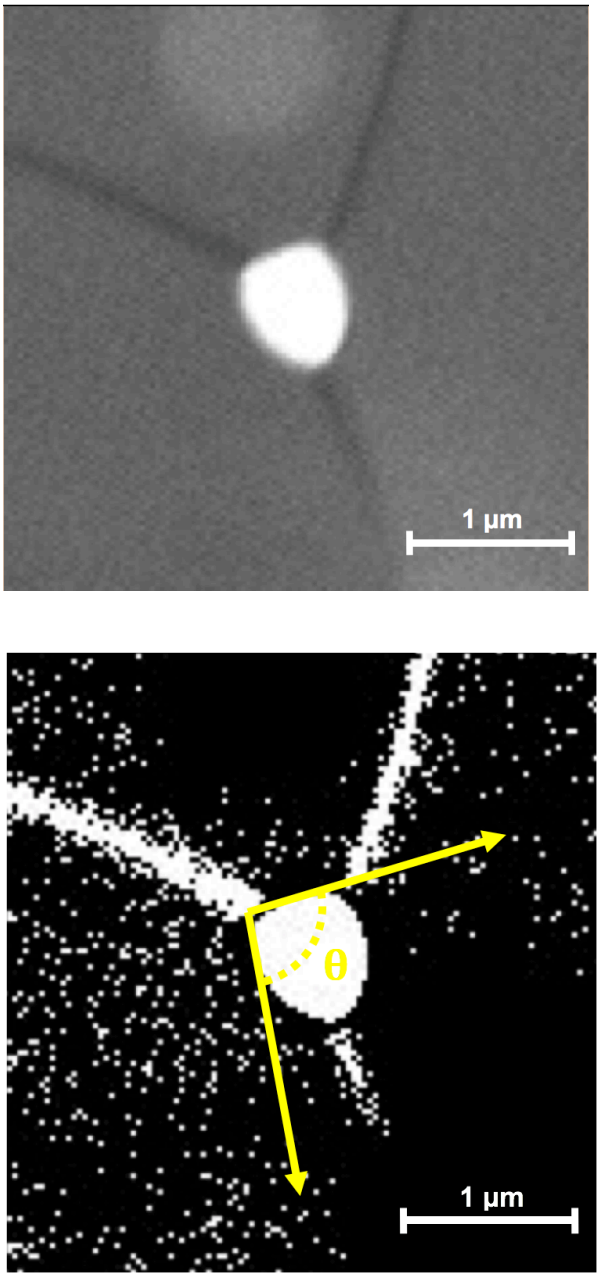

Fig. 2 Illustration of the procedure to measure apparent dihedral angle.

(a) Back scattered electron (BSE) image showing quenched Fe-C melt (bright, nearly spherical domains) at a triple junction of bridgmanite grains (gray). (b) The same BSE image in black-and-white scale, which is used to locate the separation point between adjacent grains to allow reproducible determination of apparent dihedral angle.

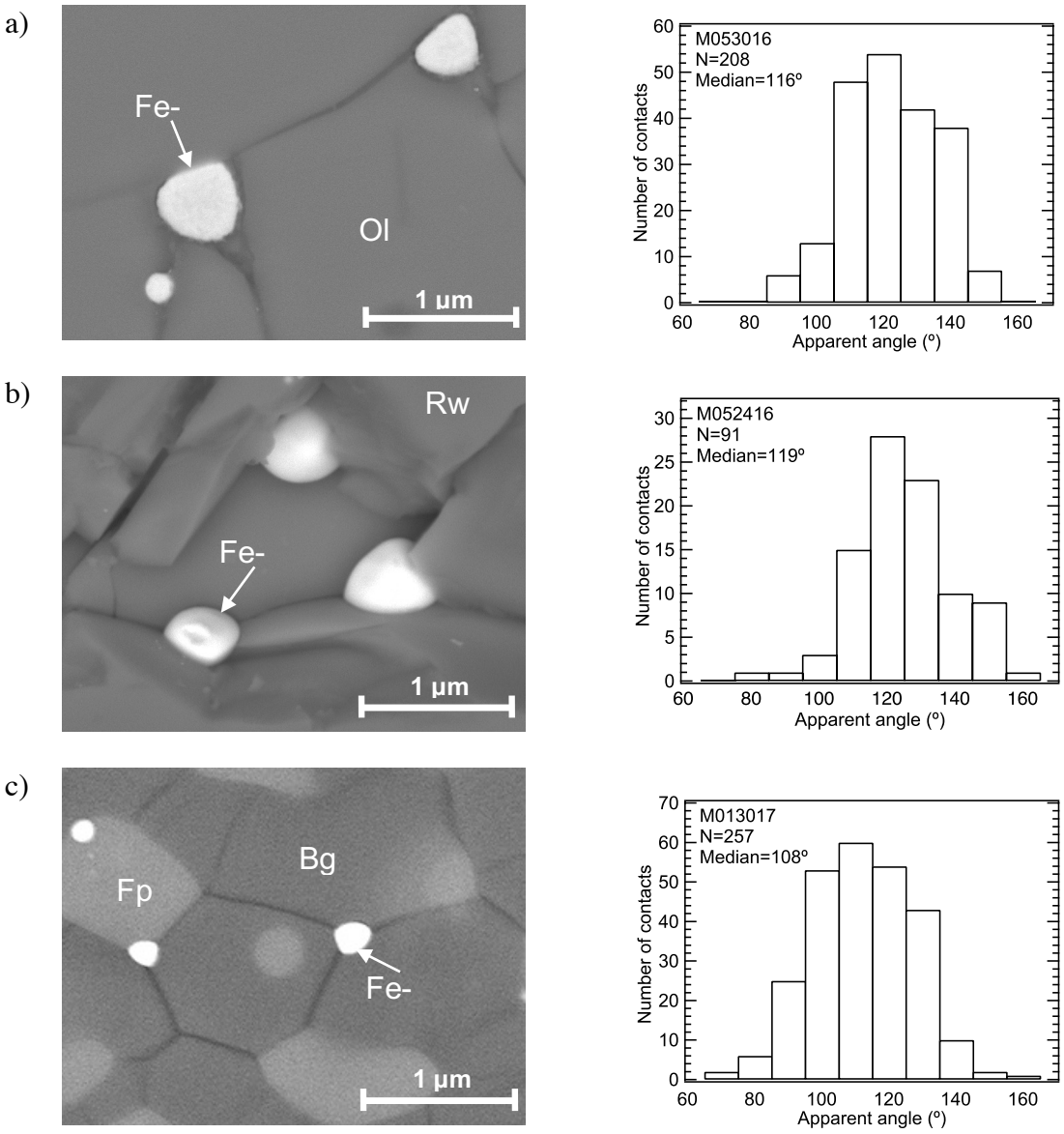

Fig. 3. Back-scattered-electron (BSE) images of experimental products and distributions of apparent dihedral angles.

(a) Experiment M053016 at 10 GPa showing quenched Fe-C melt (bright pocket) trapped in olivine matrix (gray). The median value of the apparent dihedral angles, taken as the effective dihedral angle, is 116˚. (b) Experiment M052416 at 17 GPa, showing quenched Fe-C melt (bright) in ringwoodite matrix (gray). The effective dihedral angle is 119 ˚. (c) Experiment M013017 at 23 GPa the dark grey is bridgmanite while the light gray is ferropericlase, and the effective dihedral angle, is 108˚.

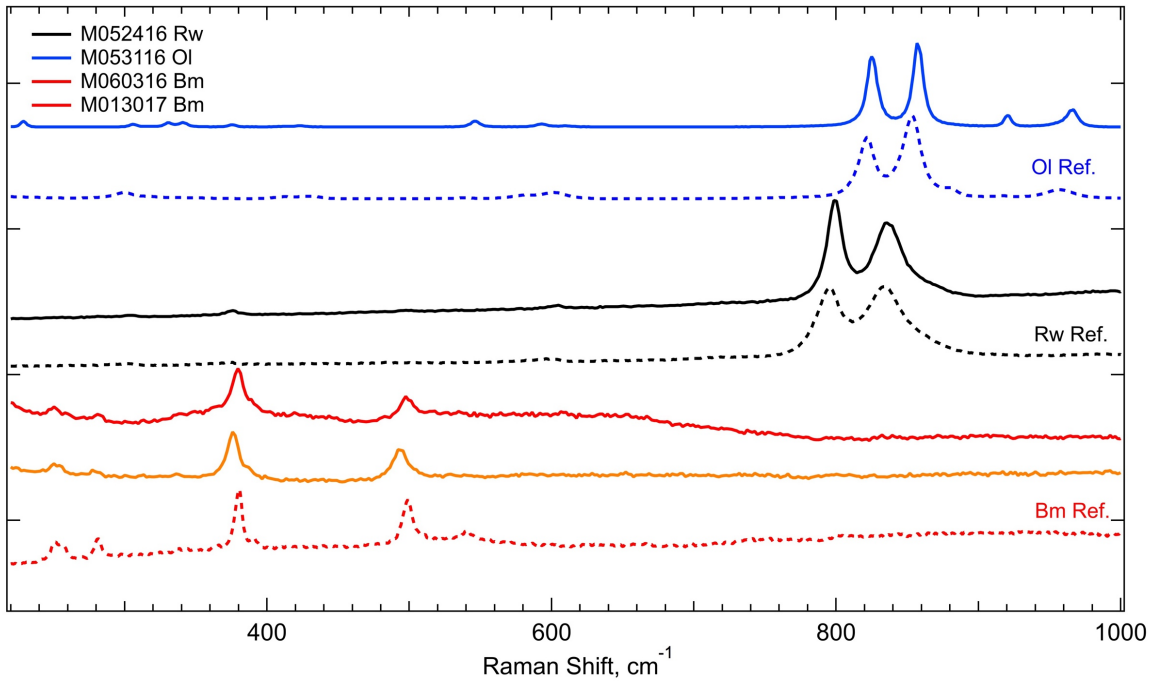

Fig. 4 (c) Raman spectra of silicate phases in experimental products. Reference spectra (dashed) for olivine (Ol), ringwoodite (Rw), and bridgmanite (Bm) are from RRUFF.

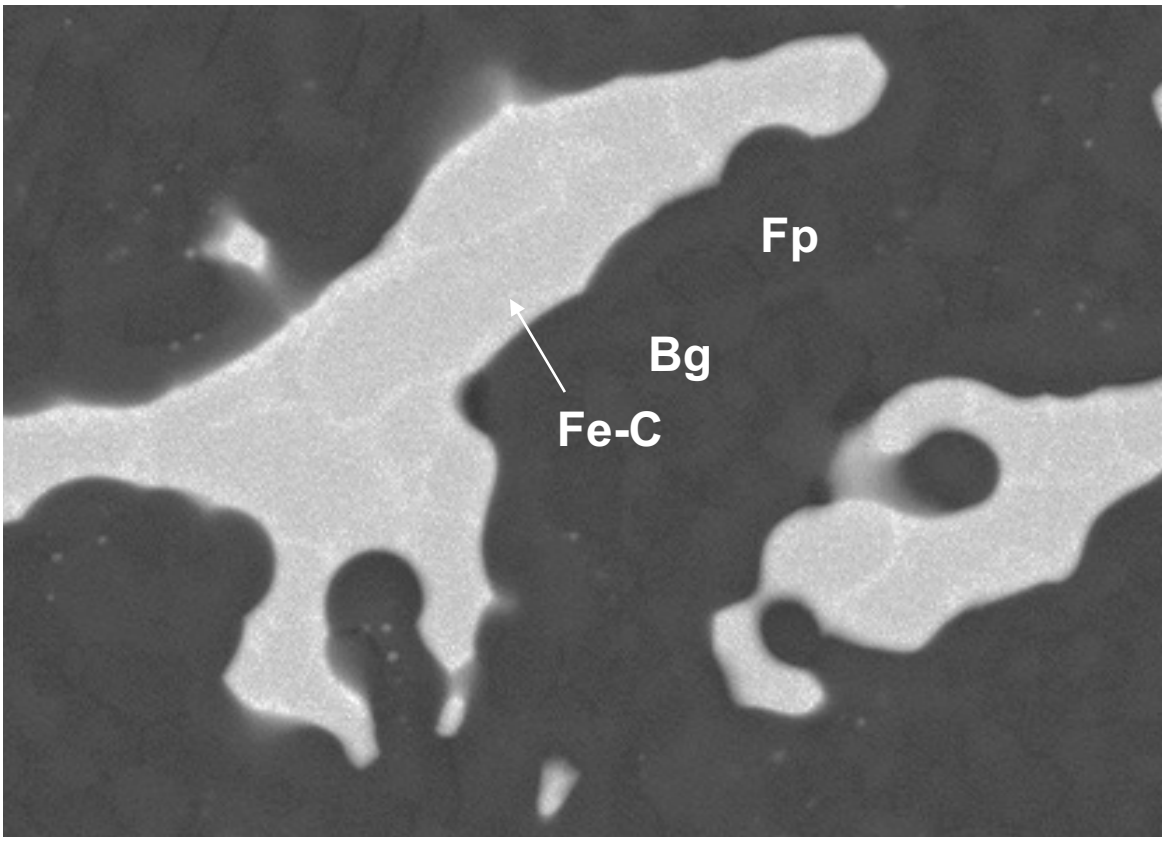

Fig. 5 Back scattered electron (BSE) image of the product of experiment M060316 at ~23 GPa showing Fe-C melt (bright) in a matrix of bridgmanite (Bg) and ferropericlase (fp). Even at an estimated volume fraction of melt at 20%, the Fe-C melt did not establish interconnectivity, suggesting a high percolation threshold.

a)

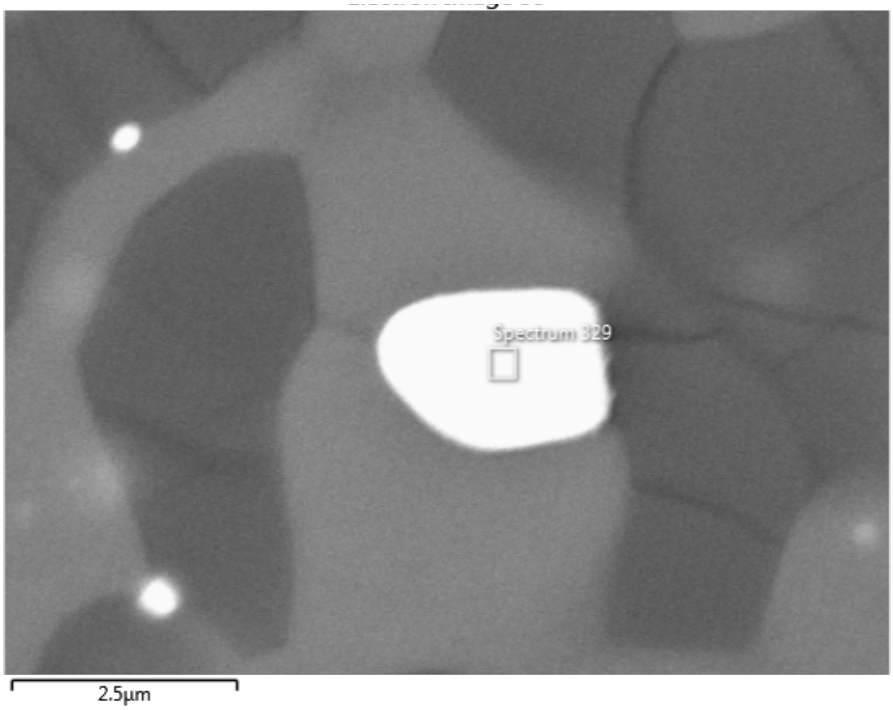

b)

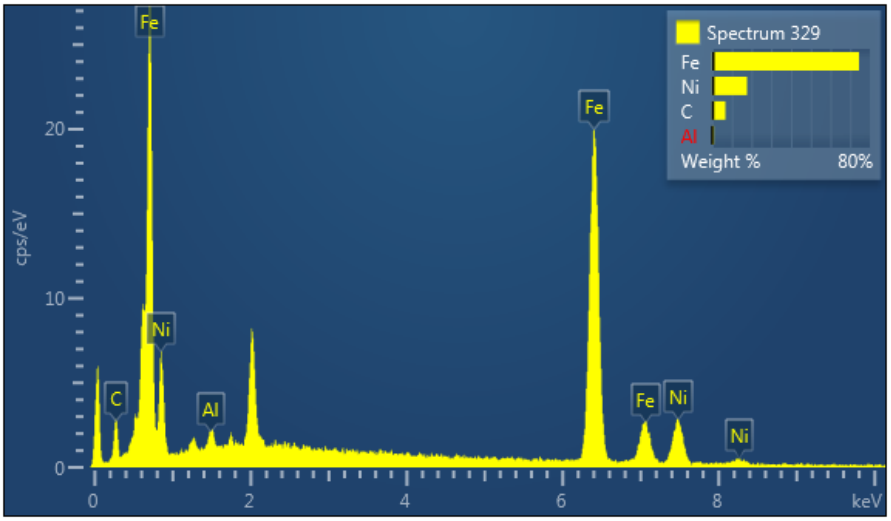

Fig. 6 Texture and composition of the product from experiment M013017.

(a) Scanning electron microscope (SEM) image, showing Fe-C melt (bright), xx (gray), and xx (dark); (b) Energy dispersive spectra (EDS) spectra of an area (gray box) in the quenched Fe-C melt with semi-quantitative chemical compositions indicated in the upper-right corner. Nickel (Ni) comes from the natural San Carlos olivine in the starting material and an aluminum (Al) peak is present because the sample was coated with Al.

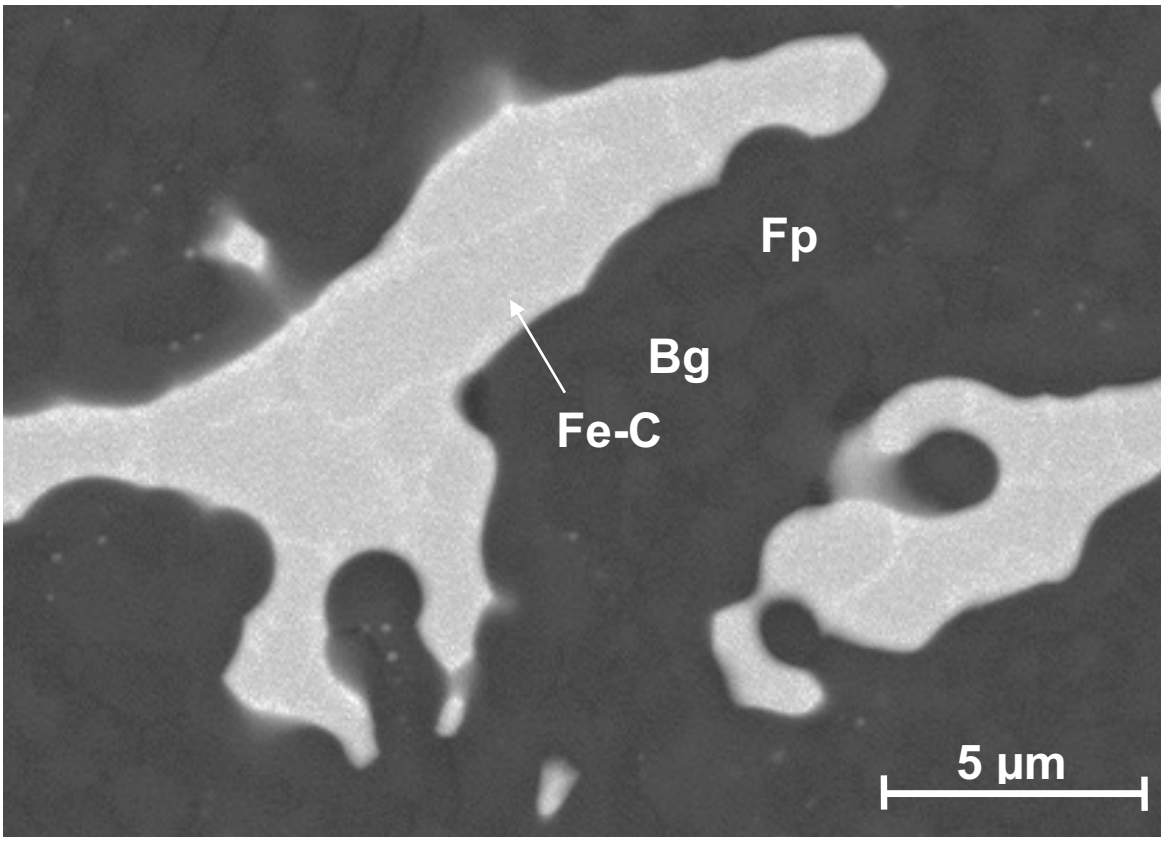

Fig. 5 Back scattered electron (BSE) image of the product of experiment M060316 at ~23 GPa showing Fe-C melt (bright) in a matrix of bridgmanite (Bg) and ferropericlase (fp). Even at an estimated volume fraction of melt at 20%, the Fe-C melt did not establish interconnectivity, suggesting a high percolation threshold.

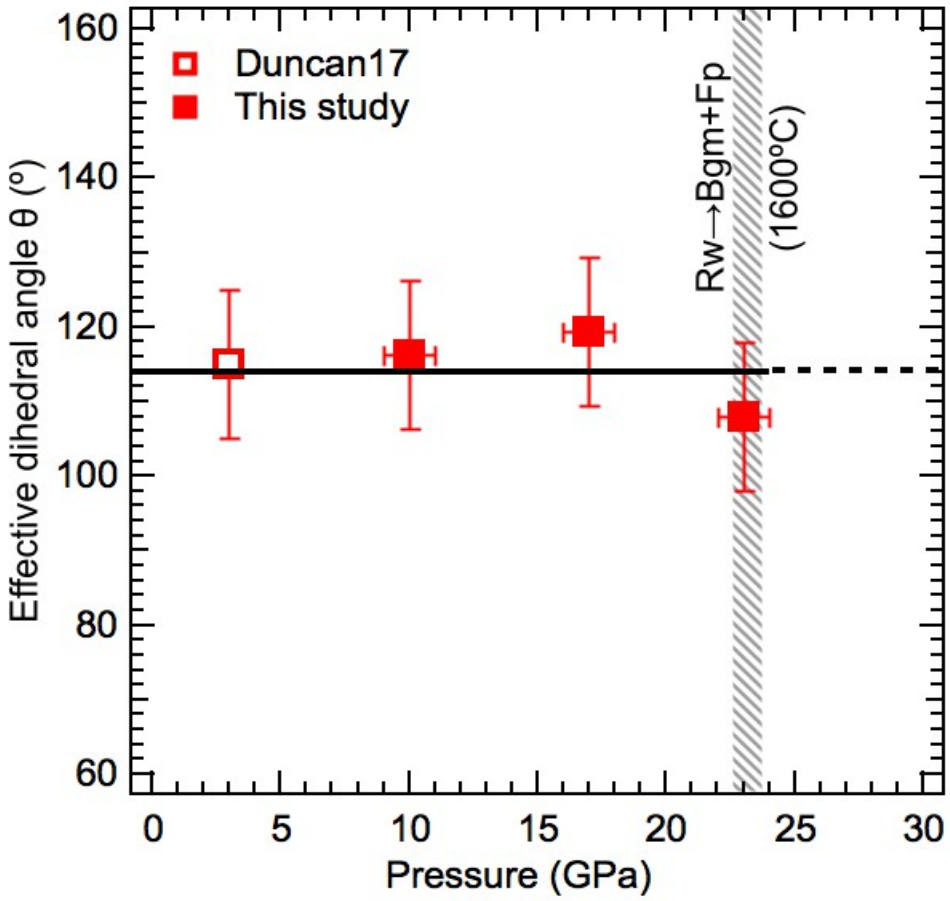

Fig. 6a Effective dihedral angle of Fe-rich melt in silicate/oxide matrix as a function of pressure.

(a) For Fe-C melt no pressure effect can be resolved within the range of 4 to 23 GPa. The open square represents a measured dihedral angle between an Fe-C melt containing 4.3 wt.% carbon (Duncan and Fei (2017)) in olivine. Solid squares are from this study. Vertical bar indicates the boundary where Ringwood (Rw) breaks down to form bridgmanite (Bgm) and ferropericlase (Fp) at 1600 ˚C.

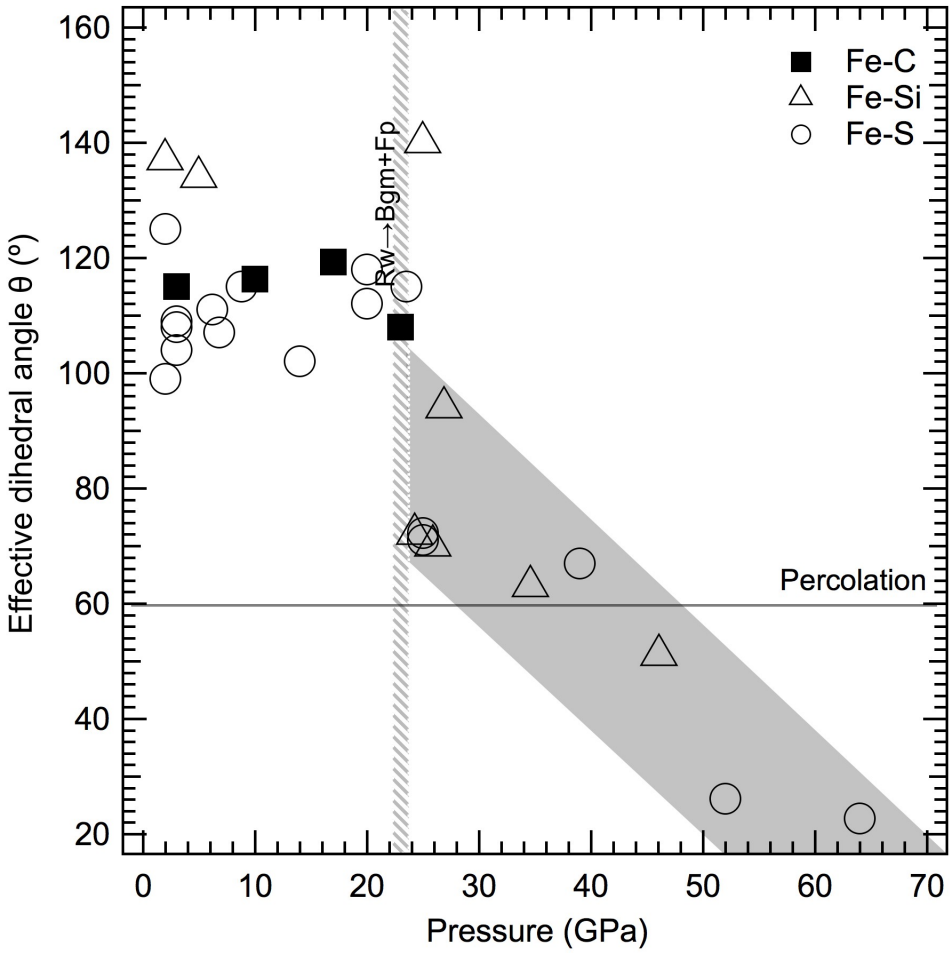

Fig. 6b Existing data on oxygen-free iron-rich melt suggest a general trend of negative pressure effect between ~25 and 64 GPa (shaded band) and no resolvable pressure effect between 1 bar and ~ 25 GPa. Data sources are: Fe-Si (open triangles, Takafuji et al. (2004, Mann et al. (2008), Fe-S (red open circles Shannon and Agee. (1996), Shannon and Agee. (1998), and Shi et al. (2013).

Table 1 Summary of experimental conditions and measurement results

Exp. ID	Pressure (GPa)[a]	Temperature[b] (°C)	Carbon content[c] (wt.%)	solid phase	# of angles measured	Dihedral angle[d] (°)
M053016	10	1600	6	olivine	208	116
M052416	17	1600	3	ringwoodite	91	119
M013016	23	1800	4	bridgmanite-ferropericlase	257	108
M060316[e]	23	1800	6	bridgmanite-ferropericlase	-	-

Duration is 30 min.

[a]Uncertainties in pressure is estimated at 2 GPa.

[b]Uncertainty in temperature is estimated ±100 °C.

[c]Carbon content is estimated from EDS spectra and semi-quantitative.

[d]Uncertainties in the measured dihedral angle is estimated at ± 10°.

[e]The sample contains a larger melt fraction, and Fe-C melt occurred as large domains with irregular shapes and did not allow determination of dihedral angle.